RSC Advances

ROYAL SOCIETY OF CHEMISTRY

www.rsc.org/advances

Cite this: DOI: 10.1039/c0xx00000x

www.rsc.org/xxxxxx

ARTICLE TYPE

Novel Magnetic Antimicrobial Nanocomposites for Bone Tissue Engineering Applications

Arundhati Bhowmick,[a] Arijit Saha,[b] Nilkamal Pramanik,[a] Subhash Banerjee,[b] Manas Das,[c] and Patit Paban Kundu*[a]

Received (in XXX, XXX) Xth XXXXXXXXX 20XX, Accepted Xth XXXXXXXXX 20XX
DOI: 10.1039/b000000x

In present study, we have demonstrated the fabrication of novel bone-like magnetic nanocomposites by the blending of chitosan, polymethylmethacrylate-co-2-hydroxyethylmethacrylate, nano-hydroxyapatite-Fe_3O_4. The hybrid nanomaterials were thoroughly characterized by Fourier transform infrared spectroscopy, powder X-ray diffraction and field emission scanning electron microscopy. The magnetic nanocomposites exhibited excellent mechanical properties (*e.g.* tensile strength, Young's modulus and stiffness) and antimicrobial activities. Hemolysis assays indicates that blood compatibility of polymer sample is significant**.** Water uptake ability of the nanocomposite materials was found to increase with increasing the proportion of PMMA-co-PHEMA. In addition, superparamagnetic nature of the nanocomposite was observed which makes these materials suitable for magnetic therapy.

1. Introduction

Development of scaffolds plays a vital role in tissue engineering in order to repair, regenerate, or create tissues and organs by mimicking of natural extracellular matrixes.[1] Scaffolds should be biodegradable, biocompatible[2] and bioresorbable having the suitable mechanical properties and the surface functionality to favor the cell adhesion, proliferation and differentiation.[3] Natural bone is composed of inorganic hydroxyapatite (HAP, $Ca_{10}(PO_4)_6(OH)_2$), and organic collagen fibrils.[4,5] To mimic natural bone, different organic-inorganic hybrid materials have been used and among these, chitosan (CTS, a natural copolymer consisting of β-[1→4]-2-acetamido-D-glucose and β-[1→4]-2-amino-D-glucose unit linkages) and HAP are the best in bone tissue engineering. This is due to the fact that CTS is biocompatible, biodegradable, and suitable for cell growth and antimicrobial in nature.[7-10] HAP is the major component (60–65%) of bone and it stimulates osteoconduction, gradually replaced by the host bone followed by implantation making it suitable for orthopedic replacements.[11] On the other hand, CTS has poor mechanical strength which restricted its practical applications in bone tissue engineering.[12] Recently, we demonstrated that the use of polymethylmethacrylate-co-2-hydroxyethylmethacrylate (PMMA-co-PHEMA) along with HAP improved the mechanical properties specifically young's modulus and stiffness[13] but the tensile strength have not been enhanced which are essential for real application in bone tissue engineering. Also scaffolds should have the antibacterial properties because in orthopedic implants bacterial infection is a predicament issue and the risk of infections frequently leading to implant failure, followed by chronic diseases. Hence, the development of scaffolds having good mechanical properties, biocompatibility and antibacterial activity is in demand for successful bone regeneration.

Literature survey reveals that nanocomposites can act as suitable candidates for bone tissue engineering as these materials responded to cell more efficiently i.e. cell proliferation and generally possessed enhanced mechanical performances.[14,15] Again,, addition of nano-HAP in natural bone improve the mechanical strength,[14] and increase the cell adhesion and proliferation of osteoblasts.[17,18]

Magnetic therapy has become a promising alternative in disease treatments especially in bone diseases. Previous report indicated that magnetic fields may stimulate the proliferation of osteoblasts, promote the expression of growth factors such as bone morphological protein, increase osteointegration, and accelerate new bone formation.[19-22] It is also advantageous to use magnetic fields to support the integration of bone and implants, to enhance bone density and calcium content, and to expedite the recovery of bone fractures.[23-26] Due to their unique magnetic properties such as biocompatibility and nontoxicity, magnetic nanoparticles have attracted mush interest. Moreover they become superparamagnetic at size below 50 nm.[27] superparamagnetic iron oxide nanoparticles (SPMNPs) have been widely used in biomedical applications such as drug delivery, magnetic resonance imaging reagents, bio-separation, enzyme immobilization, and magnetic hyperthermia,[28-31] making them suitable for in vivo applications.[32] However, their application in bone tissue regeneration has rarely been considered. Each magnetic domain provides an intrinsic magnetic therapy which further enhanced its functionality in presence of external magnetic field.[33-35] Thus, properly designed scaffold with nano

magnetic component for bone regeneration is become one of the most important subjects of research. In this connection, a few researchers have blended nano-Fe_3O_4 and HAP in presence of natural polymer (CTS or collagen) and synthetic polymer (mainly, poly-caprolactam) to improve the biocompatibility and mechanical properties respectively.[36-43]

In this paper, we demonstrated the fabrication, characterization, and study of mechanical and antimicrobial properties of bone-like magnetic nanocomposite materials simply by blending CTS, PMMA-co-PHEMA and nano-HAP-Fe_3O_4 (Scheme 1).

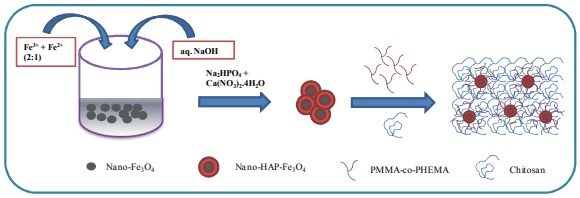

Scheme 1 Preparation of CTS/PMMA-co-PHEMA/ hydroxyapatite-Fe_3O_4 nanocomposites.

2. Experimental section

2.1 Materials

Chitosan was purchased from Acros Organics. Molecular weight of CTS was determined by the well-known Ubbelohde viscometric method and it was 230 kDa. Degree of deacetylation (DDA) of CTS was determined by potentiometric titration method and 86% DDA value was obtained. The copolymer, polymethylmethacrylate-*co*-2-hydroxyethylmethacrylate (PMMA-co-PHEMA), and nano-hydroxyapatite (nano-HAP) have been synthesized following the protocol reported in our previous paper.[13] 2-Hydroxyethylmethacrylate (HEMA) was purchased from Alfa Aesar and methylmethacrylate (MMA) was purchased from Burgoyne Urbidges and Company. HEMA monomer was purified by vacuum distillation under reduced pressure before use. The distilled HEMA monomer was then washed twice with hexanes. MMA monomer was washed with an aqueous sodium hydroxide solution, rinsed with distilled water, and dried over calcium chloride. Calcium chloride, sodium dodecylsulphate (SDS), ammonium persulphate ($(NH_4)_2S_2O_8$), glacial acetic acid, formic acid, and carboxymethylcellulose (CMC) were purchased from Merck India Ltd. SDS and $(NH_4)_2S_2O_8$ were used as surfactant and water soluble initiator, respectively. CMC was used as a stabilizer. For the synthesis of nano-HAP, calcium nitrate tetrahydrate [$Ca(NO_3)_2.4H_2O$], diammonium phosphate [$(NH_4)_2HPO_4$], and 25% ammonium hydroxide were purchased from Merck and used. For the synthesis of iron-oxide nanoparticles ferrous ammonium sulphate $(NH_4)_2Fe_2(SO_4)_3$, ferric chloride ($FeCl_3$), sodium hydroxide (NaOH) were purchased from HiMedia Private Ltd.

2.2 Detailed experimental procedure for the synthesis of chitosan-PMMA-co-PHEMA-nano-HAP-Fe_3O_4 composite materials

2.2.1 Synthesis of Fe_3O_4 nanoparticles

Fe_3O_4 nanoparticles were synthesized by co-precipitation method.[44] Aqueous solutions $(NH_4)_2Fe_2(SO_4)_3$ and $FeCl_3$ were mixed in their respective stoichiometry (Fe(II) : Fe(III) =1:2). The mixture was kept at 80 ^oC. This mixture was added to the boiling solution of NaOH (0.5 mol. was dissolved in 200 ml of distilled water) within 10 second under constant stirring. Magnetite was formed by conversion of metal salts into hydroxides, which take place immediately, and hydroxides were transformed into ferrites. The solution was maintained at 90-95 ^oC for 1.5 h.

2.2.2 Synthesis of nano-hydroxyapatite-Fe_3O_4 (nano-HAP-Fe_3O_4)

At first, 50 mg of Fe_3O_4 nanopaticles were vigorously stirred in water to make the homogeneous mixture. Then, 100 ml 0.30 M aqueous solution of Na_2HPO_4 was added and the pH was adjusted to 10-11 using aqueous solution of NaOH. Then 100 ml 0.50 M aqueous solution of $Ca(NO_3)_2.4H_2O$ was added dropwise with vigorous stirring. It was then aged at room temperature for 24 hours. The milky solution was filtered, washed with water to make alkaline free and finally washed with ethanol. It was then dried at 80 ^oC for 2 hours. Aggregated formed were crushed by morter and pestle to get fine powder. It was then calcined at 450 ^oC for 4 hours.

2.2.3 Synthesis of chitosan-PMMA-co-PHEMA-nano-HAP-Fe_3O_4 composite materials

To synthesize the bone-like magnetic materials (BMM I–III), different weight percentage of CTS, PMMA-*co*-PHEMA and nano-HAP-Fe_3O_4 has been blended (Table I). For the synthesis of BMM I–III, different amount of CTS (55, 65, and 75 wt %, respectively were dissolved in 15 ml 100 % formic acid) and PMMA-*co*-PHEMA (40, 30, and 20 wt %, respectively) were blended using a mechanical stirrer and given amount (5 wt %) of nano-HAP-Fe_3O_4 was added drop by drop to the resulting mixture with constant stirring. Homogeneous mixture of the composites (BMM I–III) was obtained upon vigorous stirring at overnight and the resulting mixture was then transferred to polystyrene petri-dishes. Upon evaporation of formic acid at room temperature, films of composite materials were obtained, which were dried at 60^oC for 48 h.

Table 1: Classification of BMMs

Bone-Like Magnetic Materials (BMMs)	CTS (wt %)	PMMA-co-PHEMA (wt %)	Nano-HAP-Fe_3O_4 (wt %)
BMM I	55	40	5
BMM II	65	30	5
BMM III	75	20	5

2.3 Physicochemical properties

Fourier transform infrared (FT-IR) spectroscopy (FT/ IR-480) was performed in the wave number range 4000–400 cm^{-1} using a ATR-FTIR (model-Alpha, Bruker, Germany) spectrometer.

X-ray diffraction patterns of BMM I-III were obtained by using X-ray diffractometer (Goniometer Miniflex, JAPAN). The samples were tested at 30 KV and 15 mA with Cu Kα radiation. The relative intensity was recorded at an angle of 2θ of 4^o/min and in the range of 5^o to 70^o.

To investigate the water uptake abilities of BMM I-III, five replicates were used for each study. The ability of the scaffolds to take up water was carried out using the procedure described below. Dry scaffolds were weighed (W_d) and immersed in distilled water upto 24 h. Then, the scaffolds were gently blotted with filter paper to remove the excess bulk water on surface and weighed (W_w) to determine the percentage of water uptake. The percentage of water absorption (E_A) of the composites at equilibrium was calculated using Equation (1):[45]

$$E_A = [(W_w - W_d)/ W_d] \times 100 \quad \text{……. (1)}$$

2.4 Microstructure of composites

The structural morphology of HAP, copolymer and BMM I-III was examined using a field emission scanning electron microscope (FESEM) (JEOL JSM7600F). For FESEM examination, samples were sputter coated with gold using E-1010 Hitachi Ion Sputter (Made in Japan).

2.5 Mechanical properties

Mechanical properties of BMM I-III were measured using a Universal Testing Machine (UTM) of Lloyd Instruments Ltd. (Model LR01KOLPLUS, ENGLAND). The measurements were performed at room temperature and with a cross-head speed of 5 mm/min with 20-mm gauge length. Width and thickness of each sample were measured before testing. At least five specimens were tested for each sample. Tensile strength, Young's modulus, stiffness and percentage elongation at break were obtained from tensile testing. The dimensions of scaffolds were 14 mm in diameter and 0.51 mm in thickness.

2.6 Antimicrobial activities

The test bacterial cultures, *Escherichia coli* XL1B strain (gram-negative), *Lysinibacillus fusiformis* strain (gram-positive) and *Bacillus cereus* (gram-positive strain) were collected from the Department of Microbiology, University of Calcutta.

Different sets of BMM (BMM I, BMM II and BMM III) were tested for antimicrobial activity by disk diffusion method[46] against *Escherichia coli* XL1B strain (gram-negative), *Lysinibacillus fusiformis* strain (gram-positive) and *Bacillus cereus (*gram-positive). The inhibitory effect was tested on a sterilized agar plate of liquid nutrient broth medium which contains animal tissue (5.0g/l), NaCl (5g/l), beef extract (1.5g/l) and yeast extract (1.5 g/l). The broth was solidified by using 1.3g/l of agar. Approximately 10^5 colony-forming units (CFU) of each strain (gram positive and gram negative bacterial strain) was swabbed uniformly on an agar plate using sterile cotton swabs to incubate at 37^oC. Different sets of composite films were cut into spherical shaped and placed it after sterilization onto each of selected zones of the agar plate and kept for 24 hours to observe the bactericidal effect on those microorganisms at 37^oC.

2.7 Hemolysis assays

The blood hemolysis of the composite film sample (BMM I) was conducted using 5 ml of fresh human blood with an ACD medium. It was centrifuged at 3000 rpm for 10 min at 4^oC. The pellet was then washed three times with cold PBS pH 7.4 by centrifugation at 3000 rpm for 10 min at 4^oC and re-suspended in the same buffer. In first phase, BMM I (4mg/ml) prepared in PBS buffer were added to the erythrocytes and were incubated for 60 min at 37^oC in a shaking water bath. In the second phase, the immersion liquid was centrifuged at 3000 for 5 min at 4^oC and the topical density of the supernatant was read by a spectrophotometer. The positive reference (100% lysis) was blood/water mixture and the negative reference (0% lysis) a blood/ saline mixture.

2.8 Magnetization analysis

Magnetization measurements were performed by using a superconducting quantum interference device (SQUID) magnetometer. A small part of the sample material was fixed in a specially designed sample holder, which allows for cancelling background contributions to the total magnetic moment. During the measurements, the magnetic field in the superconducting coil was held constant at varying temperatures, whereas the sample was consistently moved through a pick-up coil system connected to the SQUID via a flux transformer. Magnetization data were taken at temperatures 2 K< T < 300 K using a liquid-helium cooled variable-temperature insert installed in the commercial SQUID-magnetometer set-up (MPMS, Quantum Design Inc., USA).To scale the measured magnetic moments to the amount of substance, the weight of the sample was determined carefully.

3. Results and discussion

3.1 Physicochemical properties

Physicochemical properties of materials were determined using analytical techniques and were discussed below.

3.1.1 Fourier transform infrared spectroscopy

Fourier transform infrared (FT-IR) spectroscopy is one of the best methods to examine polymer– particle interaction. A detailed comparative study of FT-IR absorption band of BCM I-III was also given in Table 2. The absorption bands of nano-Fe_3O_4 (Fig 1a) appear at 575 cm^{-1} and 580 cm^{-1} are assigned to Fe–O deformation in the octahedral and tetrahedral sites. The FT-IR spectra of nano-HAP-Fe_3O_4 (Fig. 1b) exhibit bands at 1092 cm^{-1}, 1038 cm^{-1} and 964 cm^{-1} which are the characteristic bands of phosphate stretching vibration of HAP, while the bands at 574 cm^{-1} and 580 cm^{-1} are due to Fe–O deformation of Fe_3O_4. The formation of nano-Fe_3O_4-HAP composite and their interaction are clearly indicated from FT-IR studies. The broad absorptions of nano-Fe_3O_4 at 3414, 3136 and 1601 cm^{-1} were due to the surface –

Table 2: FTIR absorption bands of chitosan, PMMA-co-PHEMA, nano-HAP, nano-Fe_3O_4, nano HAP-Fe_3O_4 and their blends

CTS[13]	PMMA-co-PHEMA[13]	Nano-HAP[13]	Nano-Fe_3O_4	Nano-HAP-Fe_3O_4	BMM I	BMM II	BMM III	Assignments
3432	3440	3571	-	-	3442	3444	3441	OH stretching
2931	2952	-	-	-	2919	2921	2919	CH aliphatic stretching
2880	2852	-	-	-	2854	2853	2857	CH aliphatic stretching
-	1730	-	-	-	1724	1725	1726	CO stretching (Ester group)
1653	-	-	-	-	1654	1656	1658	CO stretching (Amide I)
1574	-	-	-	-	1575	1574	1574	NH bending (Amide I)
1161	1243	-	-	-	1147	1147	1148	Antisymmetric vibration of C-O-C
1078	1070	-	-	-	1065	1064	1066	
-	-	1090-962	-	1092-964	1115-960	1118-964	1113-966	P-O stretching for $PO4^{3-}$
			575, 580	574,580	573, 579	571, 578	572, 579	Fe–O deformation

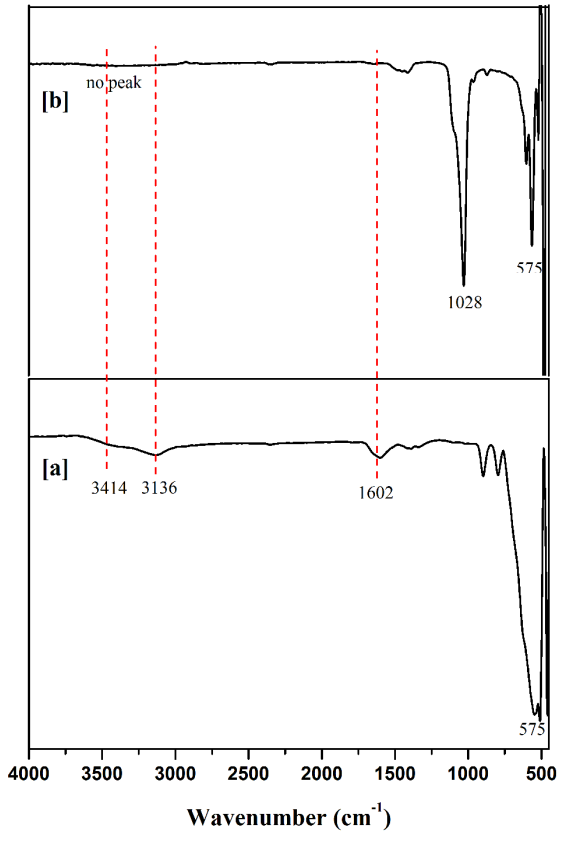

Fig. 1: FT-IR spectra of [a] nano-Fe_3O_4 [b] nano-HAP-Fe_3O_4

OH stretching and bending vibration respectively (Fig. 1a), which were absent in nano-Fe_3O_4-HAP composite (Fig. 1b). Thus –OH groups of nano-Fe_3O_4 interact strongly with phosphate groups of HAP resulting loss of peaks corresponding to –OH groups.

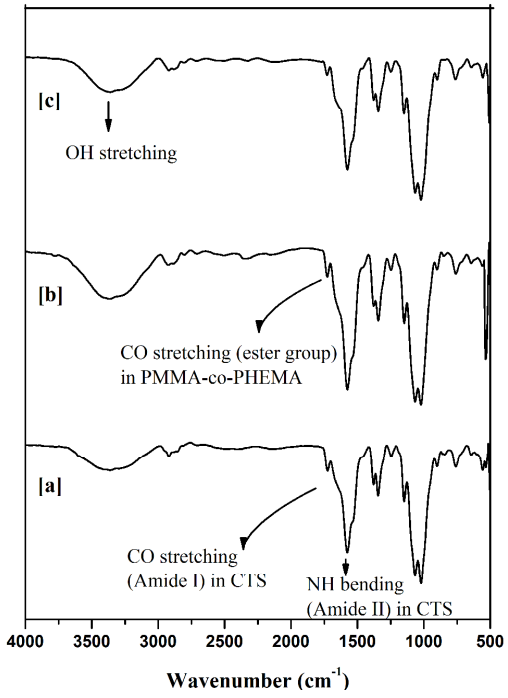

Fig. 2: FT-IR spectra of [a] BMM I, [b] BMM-II, [c] BMM III

The spectrum of BMM I, BMM II and BMM III (Fig. 2a-c) exhibits characteristic absorption bands of CTS at 1654, 1656 and 1658 cm^{-1} respectively which are attributed to amide I bands (C=O stretching mode along with an N–H deformation mode). It also showed the broad bands from 1115-960 cm^{-1}, 1118-964 cm^{-1} and 1113-966 cm^{-1}, which are the characteristic bands of phosphate (PO_4^{3-}) stretching vibration in HAP. The bands at 3442, 3444 and 3441 cm^{-1} are assigned to the hydroxyl groups present in CTS in BMM I, BMM II, BMM III respectively. Also, the presence of PMMA-PHEMA in BCM I-III was confirmed from the C=O stretching frequency due to the ester functional (-COOR) group at 1724-1726 cm^{-1} in the FT-IR absorption spectra. The characteristic peak of carbonyl stretching of pure PMMA-co-PHEMA was observed at 1730 cm^{-1},[13] a little shift of absorption peak (2-5 cm^{-1}) of C=O group occurs possibly due to the interaction between the ester group of PMMA-co-PHEMA and other polar group in nano-HAP or in CTS during blending mode of vibration.

3.1.2 Powder X-ray diffraction

The powder XRD study of the prepared nano-Fe_3O_4 (Fig. 3a) was performed and these results are in good accordance with reported values.[47] The incorporation of nano-HAP-Fe_3O_4 in CTS-PMMA-co-PHEMA composite was also evident in X-ray diffraction data (Fig. 3c-3e). From all these patterns, besides the main characteristics diffraction peaks at 2θ = 30.1°, 35.6°, 43.3°, 53.5°, 57.2° and 62.9° of the standard Fe_3O_4 crystal plane (Fig 3a), some new diffraction peaks at 2θ = 26.45° and 31.8° were also appeared, which belonged to (002) and (211) planes of crystalline HAP respectively,[33] and a broad peak at 20° was observed for CTS.

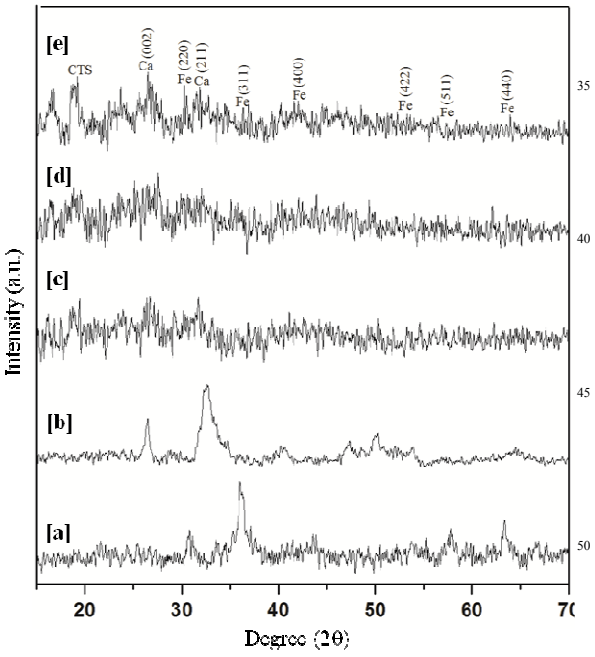

Fig. 3: XRD patterns of [a] nano-Fe_3O_4, [b] nano-HAP-Fe_3O_4, [c] BMM I, [d] BMM-II, [e] BMM III.

3.1.3 Swelling studies

Swelling studies were performed to determine the water uptake properties of the scaffolds which is one of the important properties needed for scaffolds for the application in bone tissue engineering. The bio-composite scaffolds started swelling rapidly in the first hour, indicating good characteristic property. From the results depicted in Figure 4, we can observe that with increasing the amount of PMMA-co-PHEMA (BMM III to BMM I), the water uptake ability of the composites increases in presence of fixed amount of (5 wt %) nano-HAP-Fe_3O_4. Since PHEMA introduces more hydrophilic functional groups into the copolymer, as expected the water uptake of the films were increased.

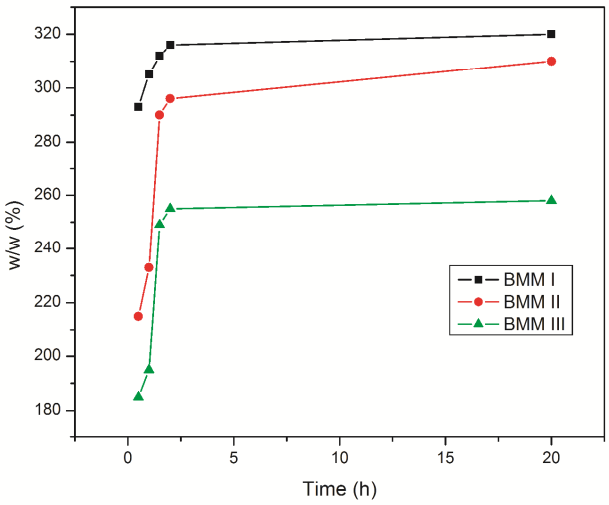

Fig. 4: Water-uptake studies of BMM I-III

3.1.4 Microstructure of composites

The size and morphology of the pure Fe_3O_4 nanoparticles were studied through the SEM analysis (Fig. 5). The size of nano- Fe_3O_4 was varied in the ranges of ~20-60 nm. The morphology of different composites (BMM I-III) was also studied through FESEM micrographs as shown in Fig. 6. From the FESEM micrographs of BMM I-III (Fig. 6) we can observe that there was a homogeneous dispersion of Fe_3O_4 nanoparticles (Fig. 6b, 6d and 6f). As we gradually increased the weight percentage of PMMA-co-PHEMA in the composites that is as we go from BMM-III to BMM-I, the structures (Fig. 6e and 6f) gradually converted to much uniform plate like structures (Fig. 6a-6d).

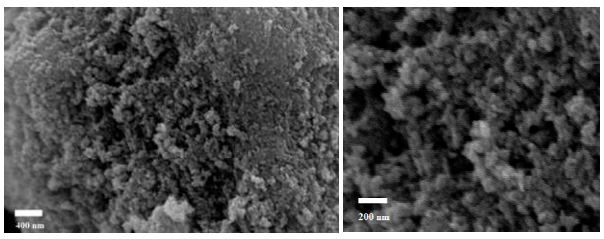

Fig. 5. Scanning-electron micrographs of nano-Fe_3O_4

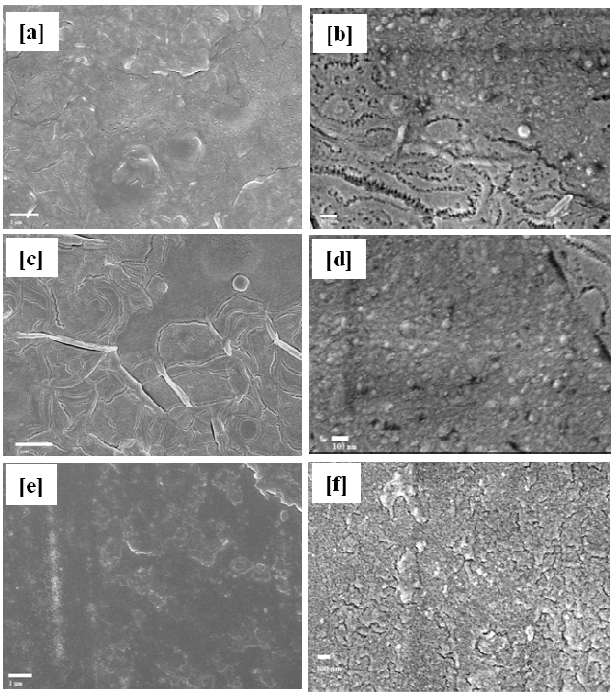

Fig. 6. Field emission scanning-electron micrographs of [a,b] BMM I, [c,d] BMM II and [e,f] BMM III

3.1.5 Mechanical properties

The tensile strength, percentage elongation at break, Young's modulus and stiffness of BMM I-III were determined and the results were listed in Table 3. In BMM I-III, the tensile strength increased dramatically with increasing content of PMMA-co-PHEMA (in presence of 5 wt % fixed amount of nano-HAP-Fe_3O_4). While with 20 wt % PMMA-co-PHEMA, BMM III has tensile strength 11.18 MPa, with 40 wt % PMMA-co-PHEMA, BMM I has 19.17 MPa of tensile strength. However, % total elongation at fracture decreased from BCM III to BMM I with the increasing content of PMMA-co-PHEMA.

Table 3: Mechanical properties of BMM I- III

	Tensile Strength (MPa)	Total Elongation at Fracture (%)	Young's Modulus (MPa)	Stiffness (N/m)
BMM I	19.17	6.31	473.66	37892
BMM II	14.37	8.92	887.83	80793
BMM III	11.18	12.54	519.21	49498

To check the effect of Fe_3O_4 nanoparticles, a control sample (BMM-IC) was prepared without nano-Fe_3O_4 by addition of 55 wt % of CTS, 40 wt % of PMMA-co-PHEMA and 5 wt % of nano-HAP. The study of mechanical properties of BMM-IC revealed that tensile strength (5.96 MPa), young's modulus (971.71 MPa) and stiffness (43079 N/m) significantly decreased in absence of nano-Fe_3O_4.

3.1.6 Antimicrobial activities

The antibacterial activity of the prepared BMM thin films was tested through the inhibition of cell growth of gram-positive and gram-negative strain. In Table 4, it was shown that with the increase in CTS contents in BMM, the inhibition of bacterial cell growth was increased and it was maximum for BMM III that contain 75 wt% of CTS. Again, the inhibition of cell growth was also found to vary for both gram-negative and gram-positive strain. For BMM III, the zone inhibition of cell growth of *Escherichia coli* XL1B, *Lysinibacillus fusiformis and Bacillus cereus* were 17±0.57 (mm), 13.6±0.57 (mm) and 15±0.57 (mm) respectively. Therefore, the BMM films were effective against

Table 4. Zone of inhibition (mm) of different sets of BMM against *Lysinibacilus fusiformis*, *Bacillus cereus* and *E.coli* XL1B strain

	Mean diameter of inhibition zone [(Mean±SD) mm] against various different sets of BMM samples		
Microorganisms	BMM I (mm)	BMM II (mm)	BMM III (mm)
Lysinibacillus fusiformis (gram-positive strain)	13.6 ±0.57	13.6 ±0.57	13.6 ±0.57
Bacillus cereus (gram-positive strain)	14.3 ±0.76	14.6 ±0.57	15.0 ±0.57
Escherichia coli XL1B (gram-negative strain)	16.6 ±0.58	17.3 ±0.57	17.0 ±0.57

gram-negative strain. However, in the case of gram-positive strain, the same inhibitory effect was comparatively lower than gram-negative strain. The exhibition of better inhibitory effect on gram-negative strain than that on gram-positive strain was due to the presence of a thicker peptidoglycan cell-wall in gram positive bacteria, protecting inner parts of the cell from the penetration of BMMs in the cytoplasm.[48] Similar kind of antimicrobial effect was observed for CTS, PMMA-co- PHEMA, nano-HAP, nano Fe_3O_4, nano-HAP-Fe_3O_4 shown in Table 5. The maximum antimicrobial activity of nano-HAP [13.0±0.76 (mm)], nano-Fe_3O_4 [17.0±0.57 (mm)], and nano-HAP-Fe_3O_4 [12.5±0.57 (mm)] was observed against *E.coli* strain. The inhibitory effect of nano-HAP against bacterial strain was in agreement with previous report.[49] Also, very smaller amount of activity against bacterial strains was reported for nano-Fe_3O_4.[50,51] Arokiyaraj et al. reported inhibition zone of nano-Fe_3O_4 against *E.coli* 7 mm only. We found better inhibition zone of nano-Fe_3O_4 against *E.coli*. The bactericidal effect of nano-Fe_3O_4 may be due to their smaller size. In summary, the CTS, PMMA-co- PHEMA and nano-HAP-Fe_3O_4 based BMM films represent a compact antimicrobial agent in biomedical field.

Table 5. Zone of inhibition (mm) of CTS, PMMA-co-PHEMA, nano-HAP, nano-Fe_3O_4 and nano-HAP-Fe_3O_4 against *Lysinibacilus fusiformis*, *Bacillus cereus* and *E.coli* XL1B strain

	Mean diameter of inhibition zone [(Mean±SD) mm] against Chitosan, PMMMA-co-PHEMA and Hydroxyapatite.				
Micro-organism	CTS (mm)	PMMA-co-PHEMA (mm)	nano-HAP (mm)	nano-Fe_3O_4 (mm)	Nano-HAP-Fe_3O_4 (mm)
Lysinibacillus fusiformis (gram-positive strain)	12.3 ±0.58	11.6 ±0.76	12.6 ±0.77	12.0 ±0.57	10.0 ±0.77
Bacillus cereus (gram-positive strain)	12.3 ±0.57	12.6 ±0.77	12.3 ±0.57	12.0 ±0.77	12.0 ±0.57
Escherichia coli XL1B (gram-negative strain)	11.3 ±0.57	10.0 ±0.78	13.0 ±0.76	17.0 ±0.57	12.5 ±0.57

3.1.7 Hemolysis assays

Hemolysis of the blood is a major problem associated with the bio-incompatibility of the polymeric material. Fig. 7 depicts the blood clotting profiles on the tested materials. The interactions of the polymeric composite film (BMM I) with negatively charged membranes have also been studied by hemolysis experiments. The release of hemoglobin was used to quantify the membrane-damaging properties of the polymers.

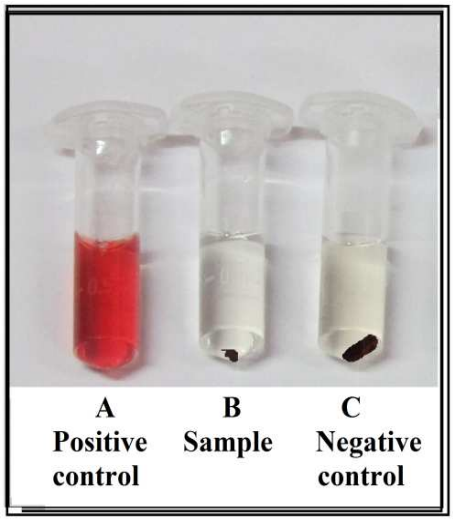

Fig. 7. The blood clotting profiles on positive control (A), sample (BMM I) (B) and negative control (C)

The positive control experiment showed that the cell membrane of hemoglobin was completely damaged in distilled water whereas in negative control experiment, the PBS buffer prohibited the hemolytic membrane from hemolysis. Again, the BMM I (4 mg/ml) was also capable to prevent the cell membrane. The percentage of hemolytic was found to 5% and it supports the blood compatibility phenomena according to reported experiment.[52] This indicates that blood compatibility of BMM I is significant and it may be appreciated the protein adsorption on the surface of sample for biomedical application.

3.1.8 Magnetization analysis

Fabrication of magnetic scaffolds for tissue engineering has been made to get benefit from a magnetic field for tissue-regeneration process. Although the magnetic guiding process is used in nanomedicine such as drug delivery and hyperthermia treatment of tumours, this concept applied in the field tissue engineering is new. Therefore, as a step towards this process, magnetic measurement was carried out in terms of magnetization. Two different measurement modes were used to perform a magnetic characterization of the sample: measurements of the field dependence of the magnetization M (H, T) at body temperature (T = 300 K) and measurements of its temperature dependence in a field (H = 200 Oe).

The temperature dependence of the magnetization of BMM I is shown in Fig. 8. The data were taken in a zero-field-cooling–field-heating sequence. The observed blocking temperature (T_B) deduced from this measurements is 172 K. More interesting, another transition at lower temperature (8 K) was also observed. Magnetization first decreases as the temperature rises from 2 K, reaches a minimum near critical phase transition temperature (T_C) of 8 K, and starts increasing from this point to the blocking temperature T_B at 172 K.

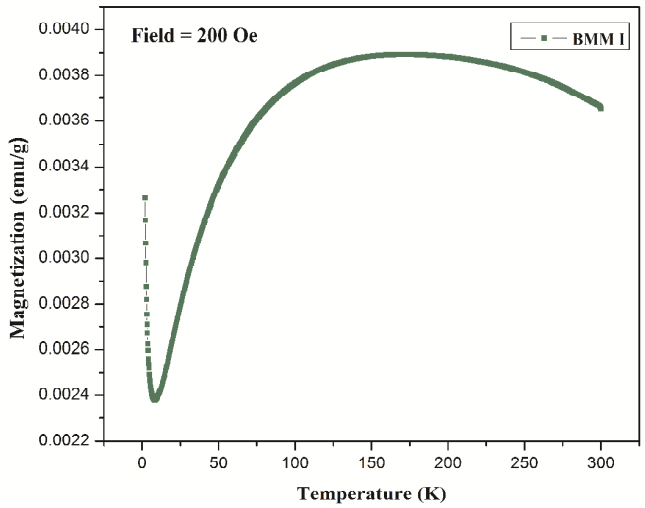

Fig. 8. Temperature dependence of the magnetization of BMN I

The results of the field-dependent magnetization measurement of BMM I is depicted in Fig. 9. Magnetization (emu/g) as a function of applied field (Oe) is depicted in with the confined field from -10000 to 10000 Oe. The coercive field of the sample took a value of 21.5 Oe at body temperature, indicative of very small

interactions between the nanoparticles. The magnetization curves are superimposed by a diamagnetic background derived from the CTS-PMMA-co-PHEMA and nano-HAP-Fe_3O_4. Spontaneous remanent magnetization was observed at 6 x 10^{-4} emu/g. This type of magnetic behavior previously observed by Santis *et al*. where they found superparamagnetic nature of poly(1-caprolactone)/iron doped hydroxyapatite (FeHA) by varying the FeHA content (10-30 wt %) in the composites.[53] In our study, superparamagnetic property with good magnetization value was observed even with very small weight percentage of nano-Fe_3O_4 (less than 1 wt %) in the nanocomposites.

Above results of these measurements confirmed the superparamagnetic character of the nanocomposite containing nano-Fe_3O_4 indicated by a very low coercive field and a distinct saturation magnetization. Thus, these nanocomposites have the capability to provide suitable magnetic therapy for bone tissue regeneration.

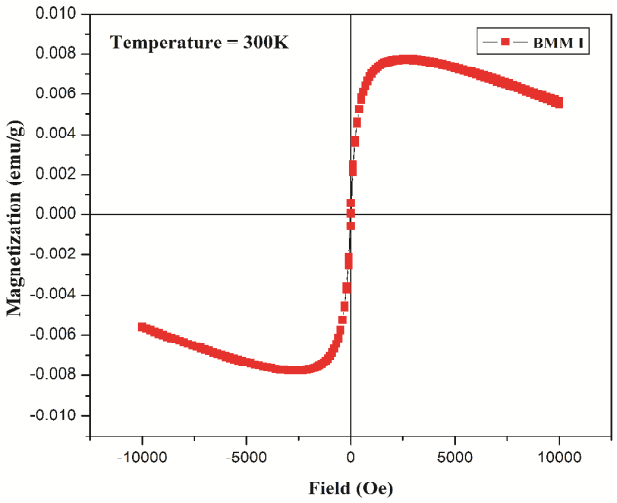

Fig. 9. Field dependent magnetization of BMN I

4. Conclusion

In conclusion, novel bone-like magnetic materials (BMM I-III) have been prepared simply by blending bio-compatible and bio-degradable natural polysaccharide of chitosan, polymethylmethacrylate-co-2-hydroxyethylmethacrylate, and hydroxyapatite-Fe_3O_4. The hybrid nano-materials were thoroughly characterized by using spectroscopic and analytical techniques. The presence of individual components was confirmed by FT-IR studies and X-ray diffraction study. The water uptake ability of the BMMs was found to increase with increasing the PMMA-co-PHEMA content. From the FESEM study, we may conclude that in presence of PMMA-co-PHEMA, composites revealed well-dispersed plate-like structure and also dispersion of nano-HAP-Fe_3O_4 in the composites is good. The study of mechanical properties revealed that the tensile strength, young's modulus and stiffness increased dramatically in BMM I where PMMA-co-PHEMA content is greater than BMM II and BMM III. Antimicrobial activities revealed that these nanocomposites have excellent antimicrobial properties which are necessary for practical applications. Also, hemolysis assays indicates that blood compatibility of polymer sample is significant. In addition, superparamagnetic nature of the nanocomposite was observed which makes these materials suitable for magnetic therapy. Thus, these materials should be potential materials for bone tissue engineering.

Notes and references

[a]Department of Polymer Science and Technology, University of Calcutta, 92 A.P.C. Road, Kolkata-700009, India.

[b]Department of Chemistry, Guru Ghasidas Vishwavidyalaya, Bilaspur, Chhattisgarh - 495009, India

[c]Department of Chemical Engineering, University of Calcutta, 92 A.P.C. Road, Kolkata-700009, India.

*Corresponding author. Email- ppk923@yahoo.com.

Phone: +91-33-2352-5106.

Electronic Supplementary Information (ESI) available: Preparation procedure, powder XRD and FT-IR spectram of control sample (BMM-IC) are given. See DOI: 10.1039/b000000x/

1 R. Langer and J. P. Vacanti, *Science*, 1993, **260**, 920.
2 M. T. Raimondi, M. Moretti, M. Cioffi, C. Giordano, F. K. Lagana and R. Pietrabissa, *Biorheology*, 2006, **43**, 215.
3 Z. K. Zhong and X. Z. S. Sun, *Polymer* 2001, **42**, 6961.
4 C. Du, F. Z. Cui, W. Zhang, Q. L. Feng, X. D. Zhu and K. D. Groot, *J. Biomed. Mater. Res. A*, 2000, **50**, 518.
5 M. Kikuchi, S. Itoh, S. Ichinose, K. Shinomiya and J. Tanaka, *Biomaterials*, 2001, **22**, 1705.
6 P. Madhavan and K. Nair, *Fish Technol*., 1974, **11**, 50.
7 K. Ogawa, S. Hirano, T. Miyanishi, T. Yui and T. A. Watanabe, *Macromolecules*, 1984, **17**, 973.
8 K. Okuyama, K. Noguchi, Y. Hanafusa, K. Osawa and K. Ogawa, *Int. J. Biol. Macromol.*, 1999, **26**, 285.
9 Sionkowska, *Prog. Polym. Sci.*, 2011, **36**, 1254.
10 S. Nath, A. Dey and B. Basu, *Mater. Sci. Eng*, 2009, **513**, 197.
11 R. Jayakumar, M. Prabaharan, S.V. Nair, S. Tokura, H. Tamura and N. Selvamurugan, *Prog. Mater. Sci.*, 2010, **55**, 675.
12 N. Shanmugasundaram, P. Ravichandran, P. Reddy, N. N. Ramamurthy, S. Pal and K. P. Rao, *Biomaterials*, 2001, **22**, 1943.
13 A. Bhowmick, R. Kumar, M. Das and P. P. Kundu, *Adv. Polym. Tech.*, 2013, **33**, 1391.
14 A. Gloria, R. De Santis and L. Ambrosio, *J. Appl. Biomater. Biomech.*, 2010, **8**, 57.
15 M. R. Rogel, H. Qiu and G. A. Ameer, *J. Mater. Chem.* 2008, **18**, 4233.
16 R. A. A. Muzzarelli, V. Baldassarre, F. Conti, P. Ferrara and G. Biagini, *Biomaterials*, 1988, 9, 247.
17 T. J. Webster, C. Ergun, R. Doremus, R. Siegel and R. Bizios, *J. Biomed. Mater. Res.*, 2000, **51**, 475.
18 T. J. Webster, C. Ergun, R. H. Doremus, R. W. Siegel and R. Bizios, *Biomaterials*, 2000, **21**, 1083.
19 C. A. Bassett, M. Schink-Ascani and S. M. Lewis, *Clin Orthop Relat Res*., 1989, **246**, 172.
20 M. T. Santini, G. Rainaldi, A. Ferrante, P. L. Indovina, P. Vecchia and G. Donelli, *Bioelectromagnetics*, 2003, **24**, 327.
21 K. J. McLeod and L. Collazo, *Radiat Res*., 2000, **153**, 706.
22 J. H. Jansen, O. P. van der Jagt and B. J. Punt, *BMC Musculoskelet Disord*., 2010, **11**, 188.
23 M. Fini, R. Cadossi and V. Canè, *J Orthop Res*., 2002, **20**, 756.
24 X. Y. Zhang, Y. Xue and Y. Zhang, *Bioelectromagnetics*, 2006, **27**, 1.
25 K. Chang and W. H. Chang, *Bioelectromagnetics*, 2003, **24**, 189–198.
26 K. F. Taylor, N. Inoue, B. Rafiee, J. E. Tis, K. A. McHale and E. Y. Chao, *J Orthop Res*., 2006, **24**, 2.

27 S. Sun, H. Zeng and D. B. Robinson, *J Am Chem Soc*., 2004, **126**, 273.
28 L. Wang, Z. Yang and J. Gao, *J Am Chem Soc*., 2006, **128**, 13358.
29 J. Kim, J. E. Lee and J. Lee, *J Am Chem Soc*., 2005, **128**, 688.
30 Y. W. Jun, Y. M. Huh and J. S. Choi, *J Am Chem Soc*., 2005, **127**, 5732.
31 O. Bretcanu, E. Verné, M. Cöisson, P. Tiberto and P. Allia, *J Magn Magn Mater*., 2006, **305**, 529.
32 R. B. Campbell, *Nanomedicine*, 2007, **2**, 649
33 Y. W. Jun, J. W. Seo and J. Cheon, *Acc. Chem. Res.*, 2008, **41**, 179.
34 U. Jeong, X. Teng, Y. Wang, H. Yang and Y. Xia, *Adv. Mater.*, 2007, **19**, 33.
35 A. K. Gupta and M. Gupta, *Biomaterials*, 2005, **26**, 3995.
36 Y. Wei, X. Zhang and Y. Song, *Biomed. Mater.*, 2011, **6**, 055008.
37 J. Meng, Y. Zhang and X. Qi, *Nanoscale*, 2010, **2**, 2565.
38 M. Bañobre-López, Y. Piñeiro-Redondo and R. De Santis, *J. Appl. Phys.*, 2011, **109**, 07B313.
39 C. Wu, W. Fan and Y. Zhu, *Acta Biomater.*, 2011, **7**, 3563.
40 A. Tampieri, E. Landi and F. Valentini, *Nanotechnology*, 2011, **22**, 015104.
41 A. Tampieri, T. D'Alessandro and M. Sandri, *Acta Biomater.*, 2012, **8**, 843.
42 R. De Santis, A. Gloria and T. Russo, *J. Appl. Polym. Sci.*, 2011, **122**, 3599.
43 N. Bock, A. Riminucci, C. Dionigi, A. Russo, A. Tampieri, E. Landi, V. A. Goranov, M. Marcacci and V. Dediu, *Acta Biomater.,* 2010, **6**, 786.
44 Y. S. Kang, S. Risbud, J. F. Rabolt, P. Stroeve, *Chem. Mater.*, 1996, **8**, 2209.
45 H. Liu, J. Mao, K. Yao, G. Yang, L. Cui and Y. Cao, *J. Biomater. Sci. Polym. Ed.*, 2004, **15**, 25.
46 V. Deepak, P. S. Umamaheshwaran, K. Guhan, R. A. Nanthini, B. Krithiga, N. M. H. Jaithoon and S. Gurunathan, Colloids and Surfaces B: Biointerfaces **2011**, 86, 353–358.
47 C. Huang, Y. Zhou, Z. Tang, X. Guo, Z. Qian and S. Zhou, *Dalton Trans.*, 2011, **40**, 5026.
48 S. Kundu, M. Mandal, S. K. Ghosh and T. Pal, *J. Colloid Interface Sci.* 2004, **272**, 134.
49 C. Deepa, A. Nishara Begum and S. Aravindan, *Nanosist.: Fiz. Him. Mat.* 2013, 4 (3), P. 370–377.
50 N. Tran, A. Mir, D. Mallik, A. Sinha, S. Nayar and T. J. Webster, *Int. J. Nanomed.* 2010, **5**, 277.
51 S. Arokiyaraj, M. Saravanan, N. K. Udaya Prakash, M. Valan Arasu, B. Vijayakumar and S. Vincent, *Mat. Res. Bull.,* 2013, **48**, 3323.
52 M. J. Parnham and H. Wetzig, *Chem. Phys. Lipids.*, 1993, **64**, 263.
53 A. Gloria, T. Russo, U. D'Amora, S. Zeppetelli, T. D'Alessandro, M. Sandri, M. Banobre-Lopez, Y. Pineiro-Redondo, M. Uhlarz, A. Tampieri, J. Rivas, T. Herrmannsdorfer, V. A. Dediu, L. Ambrosio, R. De Santis, *J R Soc Interface*, 2013, **10**, 20120833.

Novel Magnetic Antimicrobial Nanocomposites for Bone Tissue Engineering Applications

Arundhati Bhowmick, Arijit Saha, Nilkamal Pramanik, Subhash Banerjee, Manas Das, and Patit Paban Kundu

Graphical Abstract: In present study, bone like magnetic nanocomposites were fabricated by the blending of chitosan, polymethylmethacrylate-co-2-hydroxyethylmethacrylate, nano-hydroxyapatite-Fe_3O_4 and were thoroughly characterized by fourier transform infrared spectroscopy, powder X-ray diffraction and field emission scanning electron microscopy. The magnetic nanocomposites exhibited excellent mechanical properties, water uptake ability and antimicrobial activities. Hemolysis assays indicates that blood compatibility of polymer sample is significant**.** In addition, superparamagnetic nature of the nanocomposite was observed which makes these materials suitable for magnetic therapy.